LASER & PHOTONICS REVIEWS
www.lpr-journal.org

Angle-Insensitive Spectral Imaging Based on Topology-Optimized Plasmonic Metasurfaces

Jiawei Yang, Kaiyu Cui, Yidong Huang,* Wei Zhang, Xue Feng, and Fang Liu*

On-chip spectral imaging based on engineered spectral modulation and computational spectral reconstruction provides a promising scheme for portable spectral cameras. However, the angle dependence of modulation units results in the angle sensitivity of spectral imaging, which limits its practical applications. Here, metal is utilized instead of dielectric materials to realize on-chip angle-robust computational spectral imaging based on a group of topology-optimized plasmonic metasurface units under a 30° field-of-view, and demonstrate angle-insensitive spectral imaging in the wavelength range of 450–750 nm for average polarization. Furthermore, it is experimentally verified that the angle-insensitive spectral filtering effects of the fabricated metasurface units, and demonstrated angle-robust spectral reconstruction with a fidelity of over 98% as well as spectral imaging for a standard color checker. This approach expands the application scale of spectral imaging, which has great potential on metal-based on-chip multimodal imaging with dimension of depth, polarization, spectrum and so on.

1. Introduction

Spectral imaging acquires images across a wide range of the electromagnetic spectrum, finding its applications in numerous fields such as astronomy,[1,2] biomedicine,[3,4] atmospheric science,[5] and art conservation.[6] The majority of spectral imaging devices are based on spatial or spectral scanning, which requires a long acquisition time and may produce undesirable artifacts for motional objects. While for snapshot spectral imagers, real-time dynamic spectral image information can be captured without moving components.[7] Besides, the increasing demand for portable or handheld spectral cameras pushes the integration and miniaturization of spectral imaging devices. Recently, computational spectral reconstruction techniques based on engineered spectral response characteristics become a research hotspot. Related schemes include quantum dots,[8,9] disordered scattering structures,[10] nanowires,[11,12] photonic crystal slabs,[13,14] and so on. Among these schemes, quantum dots and nanowires are angle-insensitive while they are not complementary metal oxide semiconductor (CMOS) compatible for large-area fabrication to achieve spectral imaging. Scattering structures are designed for in-plane propagating light, which is not suitable for spectral imaging. As for photonic crystal slabs, or metasurfaces in a more general view, they have a rich diversity of design for light control[15,16] and support CMOS-compatible fabrication, well suited for spectral imaging.[17–19] For on-chip snapshot spectral imaging, our group has previously reported a 72 × 88 pixel ultraspectral imager based on silicon metasurfaces.[18,19] However, due to the angular dispersion of the spectral modulation units, the incident angle is required to be the same for the calibration and measurement to ensure accurate spectral reconstruction, which hinders the practical applications of on-chip spectral imaging. For angle-insensitive spectral reconstruction, a large number of angle-insensitive distinctive spectral filtering functions with as low mutual correlation as possible are required.[13] The physical origin for angle-dependent spectral response is the momentum matching condition, and localized resonant modes have been proposed to realize angle robust filtering.[20–26] However, these works are based on regular shapes or structures with limited degrees of freedom, and only several angle-insensitive color filters are realized for structural colors, not able for on-chip spectral imaging.

In this work, we propose to employ topology-optimized plasmonic metasurface units to generate diverse angle-insensitive spectral response functions for computational spectral recovery. In order to expand the metasurface design space for diverse spectral responses, we get rid of the traditional methods of metasurface design based on regular shapes and develop an inverse design approach based on freeform-shaped meta-atoms. By establishing a large geometric library containing thousands of

J. Yang, K. Cui, Y. Huang, W. Zhang, X. Feng, F. Liu
Department of Electronic Engineering
Tsinghua University
Beijing 100084, China
E-mail: kaiyucui@tsinghua.edu.cn; yidonghuang@tsinghua.edu.cn
J. Yang, K. Cui, Y. Huang, W. Zhang, X. Feng, F. Liu
Beijing National Research Center for Information Science and Technology (BNRist)
Tsinghua University
Beijing 100084, China
Y. Huang, W. Zhang
Beijing Academy of Quantum Information Science
Beijing 100084, China

The ORCID identification number(s) for the author(s) of this article can be found under https://doi.org/10.1002/lpor.202400255

DOI: 10.1002/lpor.202400255

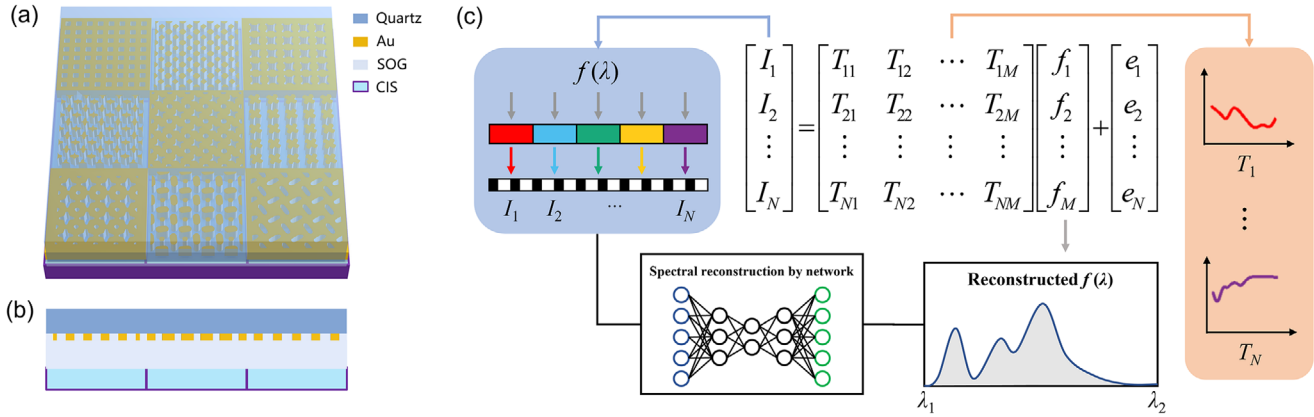

Figure 1. a) A schematic view of the proposed structure integrated with a CMOS image sensor (CIS). The structure consists of a 20-nm thick gold metasurface layer on a quartz substrate and a cover layer of spin on glass (SOG). b) The vertical section of the structure in (a). c) Principles of the computational spectral reconstruction based on the proposed structure.

different shapes with proper feature sizes and adopting a genetic algorithm, both the period and shape of the meta-atom (i.e., the unit cell of each metasurface unit) are optimized. Different from other inverse design methods[27] such as particle swarm optimization algorithm,[28] adjoint topology optimization[29–32] or deep neural network,[33–37] our method combines a global optimizer and a freeform shape generator which takes the fabrication constraints into account. As a proof of principle, we designed 100 plasmonic metasurface units using gold material for angle-robust spectral reconstruction, and further demonstrate angle-insensitive spectral imaging based on simulated spectral reconstruction using an auto-encoder. Experimentally, we fabricated a spectral imaging chip composed of 30 × 20 groups of the 100 metasurface units and calibrated the transmission spectra of the metasurface units. Furthermore, we measured the spectrum of a light emitting diode (LED) light signal under different incident angles, showing angle-insensitive spectral reconstruction, and demonstrated spectral imaging for a 24-patch Macbeth color chart. The proposed scheme has great potential for various applications of spectral imaging and provides a promising method for designing a wider variety of angle-robust devices. Besides, to the best of our knowledge, this work is the first attempt to apply metal materials instead of dielectric materials to on-chip computational spectral imaging, which can be potentially extended to ultraviolet spectral imaging,[38] multimodal imaging,[39,40] and so on.

2. Results

2.1. Structure and Principle

The schematic geometry of the proposed structure integrated with a CMOS imaging sensor (CIS) is depicted in **Figure 1**a, and the vertical section is shown in Figure 1b. An ultrathin gold metasurface layer of 20 nm is built on a quartz substrate and covered by a layer of spin on glass (SOG). The layer of SOG is used to avoid shorting with metallic pads on the CIS.[41] The plasmonic layer consists of multiple periodic array units with different periods and shapes, producing distinctive spectral response characteristics. Therefore, the photodetector underneath each metasurface unit receives a different signal from which the spectrum of incident light can be reconstructed. As shown in Figure 1c, suppose N metasurface units are used for spectrum recovery, and the unknown spectrum $f(\lambda)$ is discretized into an M-dimension vector, then the detected signals can be summarized as:

$$I = Tf + e \tag{1}$$

where I is the $N\times1$ measurement vector, T is the $N\times M$ transmission spectrum matrix, f is the $M\times1$ unknown spectrum vector, and e is the $N\times1$ measurement noise vector. The target spectrum $f(\lambda)$ can be recovered by solving Equation (1). The spectral reconstruction process can be realized by a neural network. Furthermore, the N metasurface units form a micro-spectrometer, and an array of identical micro-spectrometers can be used for spectral imaging.

For the purpose of spectral reconstruction, we need to obtain diverse spectral modulation functions by tuning the structural parameters. To break through the limitation of regular shapes in traditional metasurface design[13,14,18,21] and further expand the design space, we developed an algorithm for generating a great number of freeform shapes with controllable feature sizes (Figure S1, Supporting Information for details), and optimize both the period and shape of each meta-atom.

To explore the incident angle dependence of the metasurface units with freeform shaped meta-atoms, we simulated the angle-resolved transmission spectra of a gold hole array as shown in **Figure 2**a and a gold pillar array in Figure 2d for average polarization using Reticolo V9,[42] an open source software based on rigorous coupled-wave analysis (RCWA).[43] In the simulation, the complex refractive index of gold is taken from the data in ref.,[44] while quartz and SOG have a constant refractive index of 1.52 and 1.45, respectively. From the results in Figure 2b–e, it can be seen that the transmission spectrum almost remains the same when the incident angle varies from 0° to 30°. Furthermore, we simulated the electric field profile of the corresponding structure for the wavelength of 675 and 687 nm as shown in Figure 2c–f, respectively. For the gold hole array structure, the electric field is well confined within the hole region corresponding to a metal-insulator-metal Fabry-Perot (MIMFP) cavity mode which is an angle-independent mode.[20]

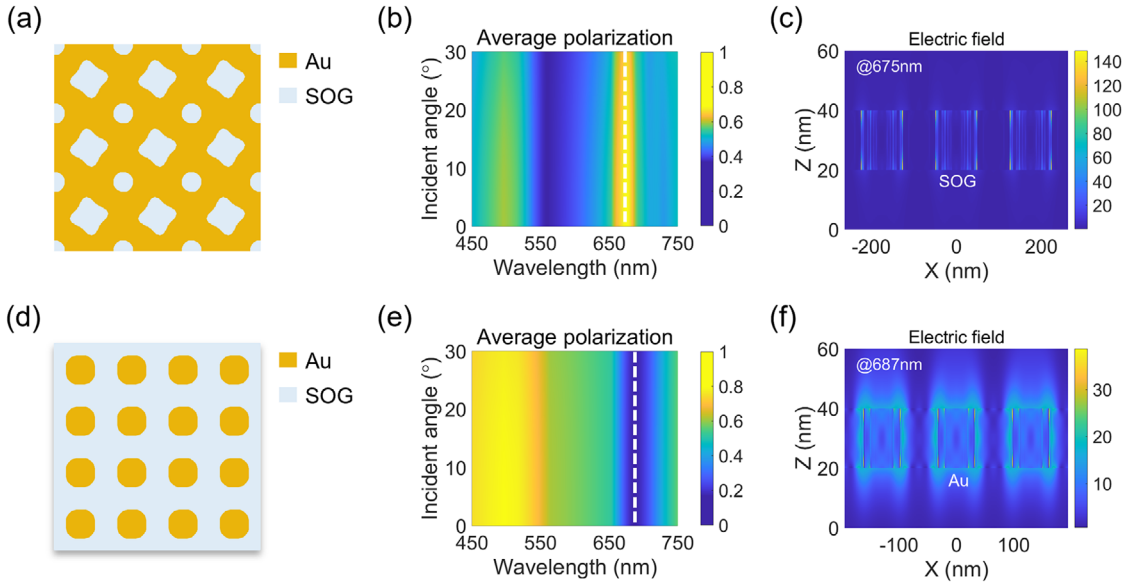

Figure 2. a) A gold hole array structure with a period of 175 nm, and b) its transmission spectra for average polarization with the incident angle varying from 0° to 30°. c) The corresponding simulated electric field distribution for the wavelength of 675 nm (indicated by the white dashed line in (b)). d) A gold pillar array structure with a period of 130 nm, and e) its transmission spectra for average polarization with the incident angle varying from 0° to 30°. f) The corresponding simulated electric field distribution for the wavelength of 687 nm (indicated by the white dashed line in (e)).

Figure 2f shows the gold pillar array structure supports localized surface plasmon resonance (LSPR) modes,[21] which is excited by appropriate polarization and frequency of the incident light regardless of the incident angle. Therefore, by introducing metal material to the structure, the localized modes such as MIMFP mode or LSPR mode can be supported while propagating modes are not dominant since they decay fast. For localized modes, the decoupling between adjacent meta-atoms makes the metasurface insensitive to the incident angle.

To obtain a group of angle-robust transmission spectra for spectral reconstruction, we set the design objective as:

$$\text{minimize} \left(\frac{1}{N}\sum_{i-1}^{N} \frac{\|T_{i1}-T_{i2}\|_1}{\|T_{i1}\|_1} - \alpha \cdot \frac{1}{N}\sum_{i=1}^{N} \min_{i\neq j} \|\tilde{T}_{i1}-\tilde{T}_{j1}\|_2 \right), \alpha > 0 \quad (2)$$

where N is the number of transmission spectra, α is the weight factor, T_{i1}, T_{i2} are the transmission spectra of the ith metasurface unit at the incident angle of 0° and 15°, respectively, and $\tilde{T}_{i1}$, $\tilde{T}_{j1}$ are the l_2-normalized transmission spectra of the ith, jth metasurface units under normal incidence, respectively. Here, the average relative difference of the transmission spectra at the incident angle of 0° and 15° is defined by the first part in Equation (2), which represents the angle sensitivity. Here, we choose an angle of 15° for a proof-of-principle demonstration, corresponding to a 30° field-of-view, which is also a typical value for most camera lenses. The second part in Equation (2) means the mean minimum mutual differences among the N spectra, which is maximized for improving the performance of spectral reconstruction.

The optimization process is illustrated in **Figure 3a**. With the aid of the shape-generation algorithm, we first build a geometric library containing thousands of freeform shapes and pick those with feature sizes larger than 50 nm with the period varying from 120 to 300 nm in a step of 5 nm. Then, the transmission spectra for all the selected shapes under each period are simulated via RCWA. After that, we apply a genetic algorithm to find the optimal N pairs of period and shape number, where a population of individuals is first initialized by random sampling, and the fitness scores of corresponding transmission spectra are calculated, followed by an iteration process of selection, reproduction, mutation and score evaluation until the fitness scores converge. The optimization process is a discrete topology optimization since the freeform shapes are not continuously varied due to the fabrication constraints.

After optimization, we obtain 100 angle-insensitive transmission spectra, two samples of which are shown in Figure 3b (the data of all samples are given in Figure S5, Supporting Information). For comparison, we randomly select 100 samples from 220-nm c-Si metasurface units with freeform-shaped meta-atoms and simulate their transmission spectra, two samples of which are shown in Figure 3c (the data of all samples are given in Figure S6, Supporting Information). As manifested in Figure 3d, the average relative difference at the incident angle of 0° and 15° (i.e., angle sensitivity) is merely 0.98% for the optimized angle-insensitive transmission spectra, while the transmission spectra for the c-Si metasurfaces exhibit an angle sensitivity as high as 23.18%. Furthermore, for the same average relative difference of 10%, the angle tolerance is up to 48° for the angle-insensitive transmission spectra, much larger than that for the angle-sensitive transmission spectra, where the angle tolerance is only 6° as indicated by the dashed line in Figure 3e. In addition, to show the generality of our method, we also designed 100 metasurface units based on silver material (Figure S2, Supporting Information for details).

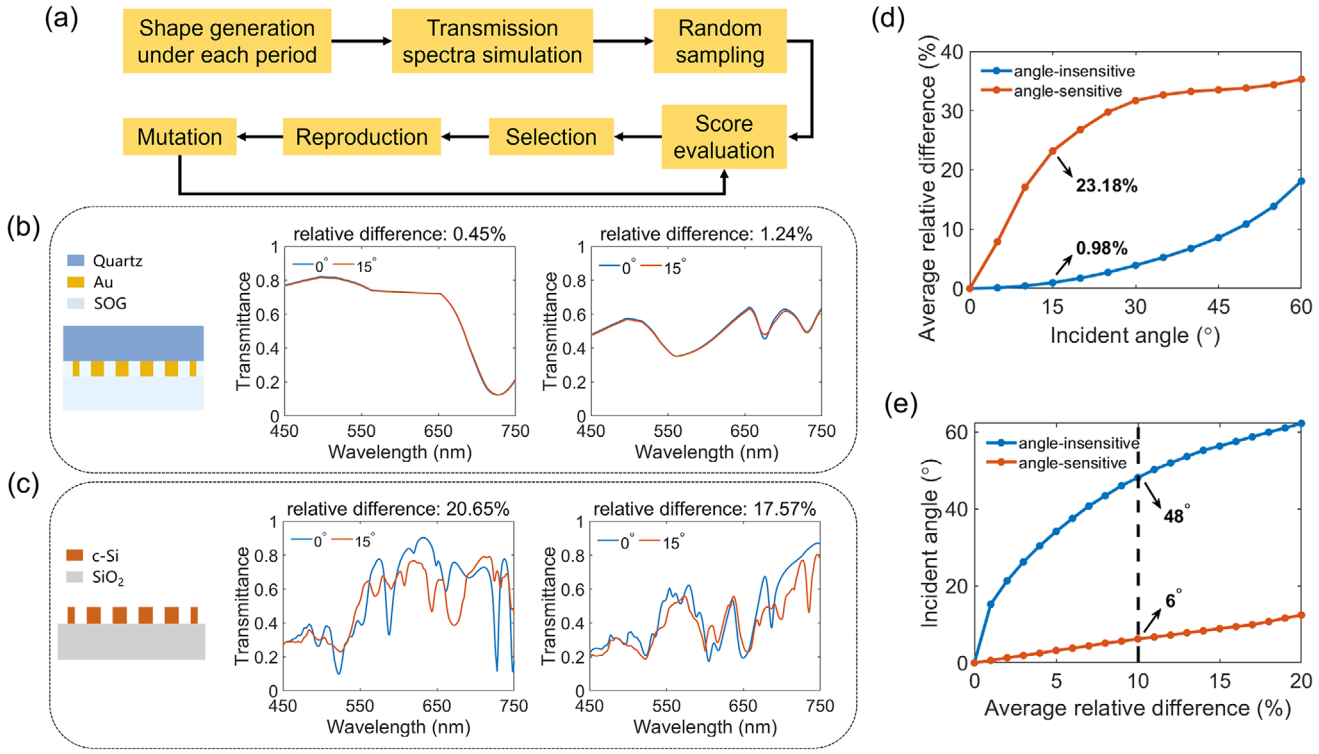

Figure 3. a) The flowchart of the optimization process with a loop of score evaluation, selection, reproduction, and mutation. b) Two samples of the optimized 100 angle-insensitive transmission spectra for the proposed structure at the incident angle of 0° and 15°. c) Two samples of the simulated transmission spectra of 100 silicon-based metasurface units at the incident angle of 0° and 15°. d) The average relative difference of the angle-insensitive and angle-sensitive transmission spectra as a function of incident angle compared with the case for normal incidence. e) The incident angle for different average relative differences of the angle-insensitive and angle-sensitive transmission spectra.

2.2. Simulated Spectral Reconstruction

Furthermore, to test the performance of spectral reconstruction using the optimized transmission spectra, we implement simulated spectral reconstruction through an auto-encoder as illustrated in **Figure** 4a, which is composed of an encoder and a decoder. Here, the encoder contains only an unbiased fully connected layer with the weight matrix corresponding exactly to the transmission spectra.[45] Therefore, the encoder plays the role of simulated measurement with the input spectrum f and output measurement vector *I*. Besides, we add Gaussian white noise[46,47] to *I* as measurement noise vector e of Equation (1). As for the decoder, it consists of three fully connected layers for spectral recovery. The number of input and output nodes for each layer is marked in Figure 4a. We build a synthetic spectral dataset for training the network, where the number of training and test sets are randomly split by a ratio of 9:1. The dataset contains 200 000 Gaussian line shape spectra, which are produced by adding a series of Gaussian distribution component functions together.[46] The network is trained for 100 epochs using Adam optimizer with a batch size of 2000. The initial learning rate is 0.001 and decays 1.25 times every 10 epochs.

To evaluate the performance of spectral reconstruction, we use a metric of fidelity defined as:

$$F(f_1,f_2) = \langle f_1,f_2 \rangle \quad (3)$$

where f_1, f_2 are the l_2-normalized original spectrum and reconstructed spectrum vector, respectively, and <> means the inner product. Under different noise levels, we train the network using the transmission spectra under normal incidence in Figure 3b,c. Then, we calculate the average fidelities of spectral reconstruction on the test set under the incident angle of 0° and 15°, using the trained network. For the optimized angle-insensitive transmission spectra, it can be seen that there is no significant reduction in the fidelities when the incident angle varies from 0° to 15° in Figure 4b, whereas the case is different for the angle-sensitive transmission spectra of c-Si metasurface units in Figure 4c.

For the demonstration of spectral imaging, we use the trained spectral auto-encoder to reconstruct the data cube of 254 × 345 × 301 for a 24-patch Macbeth color checker with 2% Gaussian white noise, where the 2% level is just an example. Figure 4d shows the post-colored image in RGB form obtained by a commercial spectral camera (Dualix Instruments, GaiaField Pro V10) as a reference. The reconstructed results using the optimized simulated transmission spectra are displayed in Figure 4e,f, where the reconstructed image hardly varies with the incident angle and shows angle-insensitive performance. As for the results in Figure 4h,i using the transmission spectra in Figure 3c, the performance of spectral imaging significantly deteriorates as the incident angle increases. Through the sampled spectra in Figure 4g–j for the point *P* in Figure 4d, it is confirmed again that the optimized transmission spectra can be used for angle-robust spectral imaging. In theory, other metals can also be

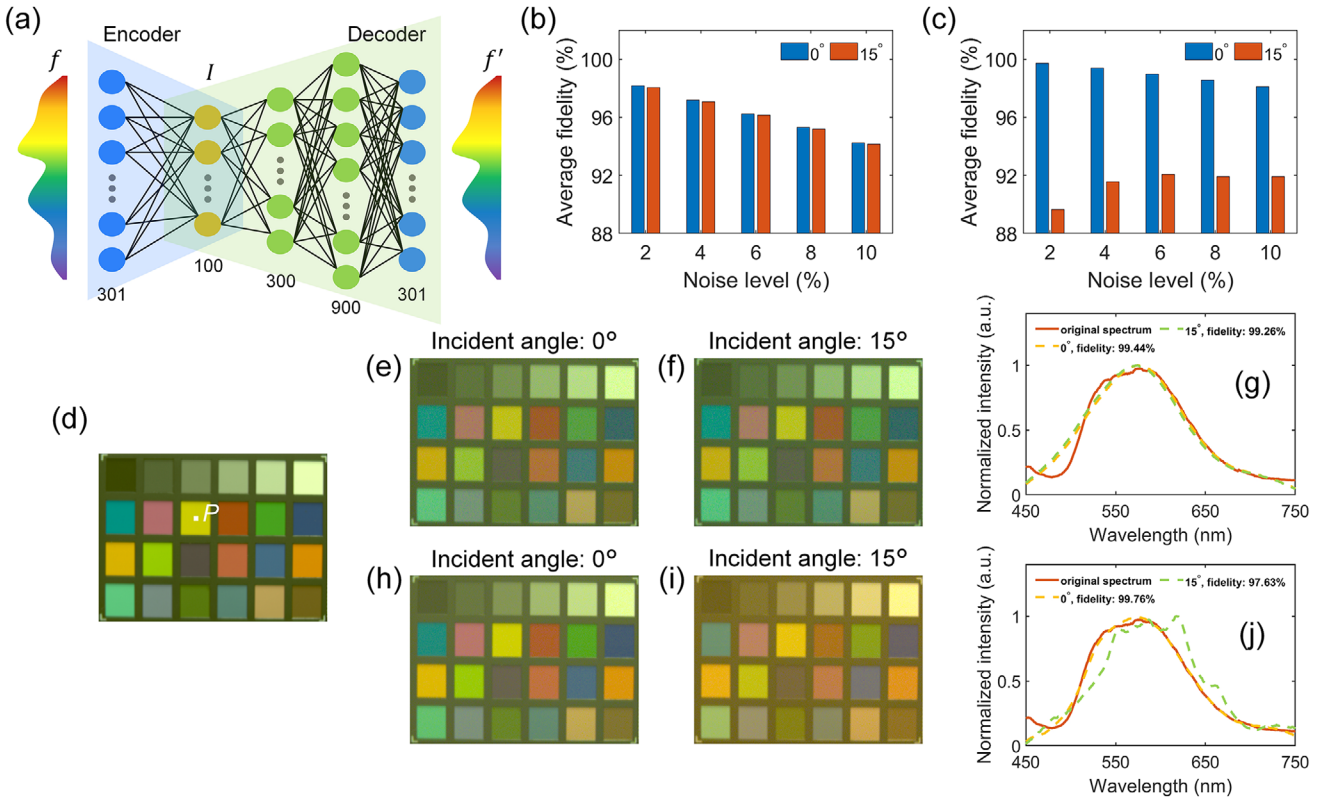

Figure 4. a) The network architecture of the auto-encoder for simulated spectral reconstruction. b,c) Average spectral reconstruction fidelity for the test spectral dataset using the transmission spectra in Figure 3b,c as the weight matrix of the encoder in (a), respectively. d) The post-colored image for a 24-patch Macbeth color chart obtained using a commercial spectral camera (Dualix Instruments, GaiaField Pro V10). e, f) and (h, i) The reconstructed post-colored images with 2% Gaussian white noise using the transmission spectra in Figure 3b,c, respectively. (e) (h) correspond to the incident angle of 0° and (f) (i) correspond to 15°. (g) and (j) Results of simulated spectral reconstruction with 2% Gaussian white noise for the point P in (d) using the transmission spectra in Figure 3b,c, respectively.

used for designing the angle-insensitive metasurface layer. The results of simulated spectral imaging using the designed silver metasurface units are provided in Figure S2 (Supporting Information).

2.3. Experimental Validation

To experimentally validate the proposed approach, we fabricated a spectral imaging chip composed of 300 × 200 gold metasurface units by arranging the 10 × 10 kinds of metasurface units repeatedly 30 × 20 times (Figure S3, Supporting Information for details). The size of each metasurface unit is 15 μm × 15 μm, covering 5 × 5 CIS pixels with a pixel size of 3 μm ×3 μm. **Figure** 5a shows the image of the packaged module of the spectral imaging chip and an optical micrograph of some metasurface units where the blue box contains 10 × 10 kinds of gold metasurface units with various colors. The scanning electron microscope images of four selected metasurface units are presented in Figure 5b. We calibrated the transmission spectra of all metasurface units at different incident angles in the wavelength range of 450–750 nm (Figure S4, Supporting Information for details). The angle-insensitive feature can be seen from the results presented in Figure 5c for the four metasurface units in Figure 5b. Quantitatively speaking, the average relative difference of the 100 calibrated transmission spectra at the incident angle of 0° and 15° is only 3.62%. To show the angle-robust spectral reconstruction, we measured the spectrum of an LED light source at the incident angle of 0° and 15°, with the reference spectrum obtained by a commercial spectrometer (OceanView QE Pro). As a comparison, we also measured the same spectrum using the 100 silicon-based metasurface units in Figure 3c. The spectra are reconstructed using the aforementioned spectral decoder trained using the calibrated transmission spectra under 2% Gaussian white noise. From the results in Figure 5d, we can see that the spectrum can be well recovered using the gold metasurface units, with fidelity over 98% even under the incident angle of 15°. In the case of silicon-based metasurface units, the reconstruction fidelity rapidly decreases by ≈2% when the incident angle increases from 0° to 15°. The performance for spectral reconstruction can be further improved by increasing the mutual differences among the 100 transmission spectra, which can be achieved by using a multilayer structure, decreasing the feature size, using other metal materials, etc.

Last but not least, we show the potential of spectral imaging using the fabricated chip. We assembled a lens with a focal length of 12 mm to the spectral imaging chip, and captured the image of a standard 24-patch Macbeth color checker under light

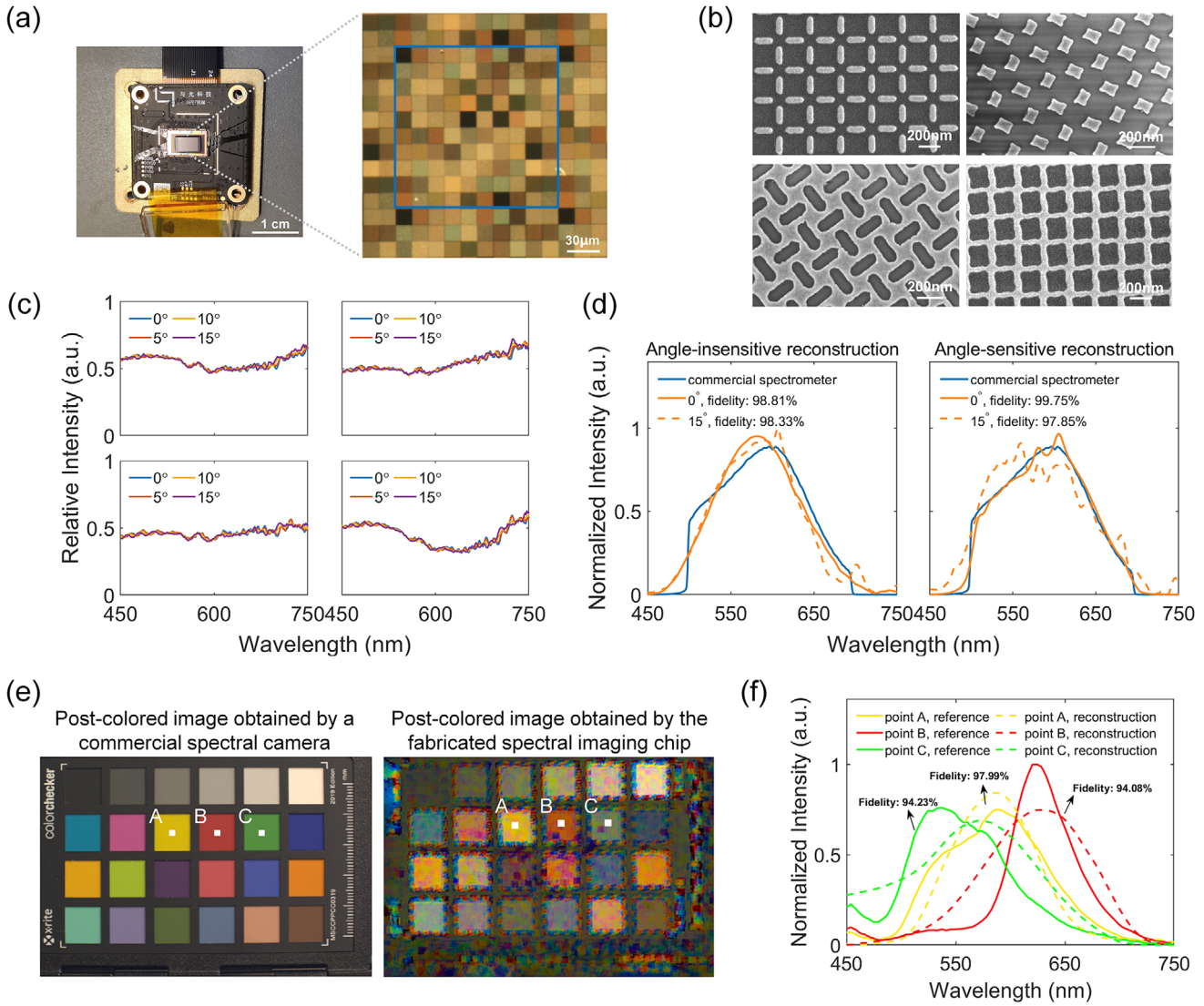

Figure 5. a) Device photograph and optical image of the fabricated spectral imaging chip. The blue box shows the 100 kinds of gold metasurface units. b) Scanning electron microscope images of four metasurface units. c) The calibrated transmission spectra of the four metasurface units in (b) at the incident angle of 0°, 5°, 10°, and 15°. d) Reconstructed results of the spectrum of an LED at the incident angle of 0° and 15° using 100 gold metasurface units and silicon-based metasurface units. e) The recovered post-colored image of a 24-patch Macbeth color chart obtained by a commercial spectral camera (Dualix Instruments, GaiaField Pro V10) and the fabricated chip in (a). f) The reconstructed spectra (dashed lines) for the selected three points in (e) with the spectra captured by the commercial spectral camera as a reference (solid lines). The fidelities for the recovered spectra are shown in the figure.

from an ordinary LED. Figure 5e gives the results of recovered post-colored RGB image of the color checker with a reference obtained by a commercial spectral camera (Dualix Instruments, GaiaField Pro V10). Figure 5f shows the results of reconstructed spectra (dashed lines) for the three sampled points marked in Figure 5e along with the reference results (solid lines). Here, we use 36 metasurface units for spectral reconstruction at each spatial point, and spatial multiplexing is utilized to enhance spatial resolution.[15,16] It can be seen that the recovered color image visually matches well with the reference result, and the reconstructed spectra for the three sampled points have a mean fidelity of 95.43%. Although the reconstructed accuracy is obviously lower than that of silicon-based metasurface spectral imaging chip[18,19] due to the relatively poor spectral modulation ability of gold metasurface units, the proposed design can be potentially used in wide-angle applications without the demand of high spectral precision such as object detection or classification.

3. Conclusion

In conclusion, we propose to utilize the topology-optimized plasmonic metasurfaces as spectral modulation units to address the sensitivity of transmission spectra to the incident angle. Through the joint optimization of the period and shape for each meta-atom, we designed 100 plasmonic metasurface units with distinctive angle-robust transmission spectra whose angle sen-

sitivity is merely 0.98%, and the angle tolerance for the average relative difference of 10% is up to 48°, which is significantly improved compared to the silicon metasurfaces. Furthermore, we test the performance of simulated spectral reconstruction by training an auto-encoder with a dataset of 200 000 synthetic Gaussian line shape spectra and demonstrate angle-insensitive spectral imaging for a standard color calibration board. Finally, we fabricated a spectral imaging chip containing 30 × 20 groups of the 100 kinds of metasurface units with a measured angle sensitivity of 3.62%. Besides, we experimentally realized angle-insensitive spectral reconstruction with a fidelity of over 98% and demonstrated spectral imaging for a standard color checker. The main limitation of this work is that the spectral reconstruction accuracy is not high due to the limited mutual differences among the transmission spectra, which can be possibly improved by using a multilayer structure, decreasing the feature size, using other metal materials, etc.

We believe that our approach has great potential to push the development and expand the application fields of on-chip spectral imaging. With larger angle tolerance, spectral imaging chips can be assembled with wide-angle lenses for large field-of-view imaging or tilt-shift lenses for off-axis imaging, and be potentially used in smartphones, digital cameras, and other consumer electronic devices. In addition, we first utilize metal instead of dielectric materials to realize on-chip computational spectral imaging, which paves the way for metal-based on-chip multimodal imaging with dimensions of depth, polarization, spectrum, and so on. Finally, beyond the field of spectral imaging, the methods of topology optimization proposed here can also be applied in other fields such as angle-insensitive structural color printing schemes,[48] angle-robust reconfigurable intelligent surface in wireless communications,[49] wide-angle electromagnetic absorbers,[50] and so on.

Supporting Information

Supporting Information is available from the Wiley Online Library or from the author.

Acknowledgements

The National Key Research and Development Program of China (2023YFB2806703 and 2022YFF1501601). The National Natural Science Foundation of China (Grant No. U22A6004); and the Beijing Frontier Science Center for Quantum Information; and Beijing Academy of Quantum Information Sciences. The authors would like to thank Tianjin H-Chip Technology Group Corporation, Innovation Center of Advanced Optoelectronic Chip and Institute for Electronics and Information Technology in Tianjin, Tsinghua University for their fabrication support with EBL and ICP etching.

Conflict of Interest

The authors declare no conflicts of interest.

Data Availability Statement

The data that support the findings of this study are available from the corresponding author upon reasonable request.

Keywords

angle-insensitivity, plasmonic metasurface, spectral imaging, topology optimization

Received: February 24, 2024
Revised: May 18, 2024
Published online:

[1] F. Gabrieli, K. A. Dooley, M. Facini, J. K. Delaney, *Sci. Adv.* **2019**, *5*, eaaw7794.
[2] S. Minardi, R. J. Harris, L. Labadie, *Astron. Astrophys. Rev.* **2021**, *29*, 29.
[3] Q. Li, X. He, Y. Wang, H. Liu, D. Xu, F. Guo, *J. Biomed. Opt.* **2013**, *18*, 100901.
[4] G. Lu, B. Fei, *J. Biomed. Opt.* **2014**, *19*, 010901.
[5] J. S. Greaves, A. M. S. Richards, W. Bains, P. B. Rimmer, H. Sagawa, D. L. Clements, S. Seager, J. J. Petkowski, C. Sousa-Silva, S. Ranjan, E. Drabek-Maunder, H. J. Fraser, A. Cartwright, I. Mueller-Wodarg, Z. Zhan, P. Friberg, I. Coulson, E. '. Lee, J. Hoge, *Nat. Astron.* **2021**, *5*, 655.
[6] H. Liang, *Appl. Phys. A* **2012**, *106*, 309.
[7] N. A. Hagen, M. W. Kudenov, *Opt. Eng.* **2013**, *52*, 090901.
[8] J. Bao, M. G. Bawendi, *Nature* **2015**, *523*, 67.
[9] X. Zhu, L. Bian, H. Fu, L. Wang, B. Zou, Q. Dai, J. Zhang, H. Zhong, *Light Sci. Appl.* **2020**, *9*, 73.
[10] B. Redding, S. F. Liew, R. Sarma, H. Cao, *Nat. Photonics* **2013**, *7*, 746.
[11] Z. Yang, T. Albrow-Owen, H. Cui, J. Alexander-Webber, F. Gu, X. Wang, T.-C. Wu, M. Zhuge, C. Williams, P. Wang, A. V. Zayats, W. Cai, L. Dai, S. Hofmann, M. Overend, L. Tong, Q. Yang, Z. Sun, T. Hasan, *Science* **2019**, *365*, 1017.
[12] J. Meng, J. J. Cadusch, K. B. Crozier, *Nano Lett.* **2019**, *20*, 320.
[13] Z. Wang, S. Yi, A. Chen, M. Zhou, T. S. Luk, A. James, J. Nogan, W. Ross, G. Joe, A. Shahsafi, K. X. Wang, M. A. Kats, Z. Yu, *Nat. Commun.* **2019**, *10*, 1020.
[14] Y. Zhu, X. Lei, K. X. Wang, Z. Yu, *Photonics Res.* **2019**, *7*, 961.
[15] T. Pertsch, S. Xiao, A. Majumdar, G. Li, *Photonics Res.* **2023**, *11*, OMFA1.
[16] W. Yang, S. Xiao, Q. Song, Y. Liu, Y. Wu, S. Wang, J. Yu, J. Han, D.-P. Tsai, *Nat. Commun.* **2020**, *11*, 1864.
[17] I. Kim, H. Kim, S. Han, J. Kim, Y. Kim, S. Eom, A. Barulin, I. Choi, J. Rho, L. P. Lee, *Adv. Mater.* **2023**, *35*, 2300229.
[18] J. Xiong, X. Cai, K. Cui, Y. Huang, J. Yang, H. Zhu, W. Li, B. Hong, S. Rao, Z. Zheng, S. Xu, Y. He, F. Liu, X. Feng, W. Zhang, *Optica* **2022**, *9*, 461.
[19] J. Yang, K. Cui, X. Cai, J. Xiong, H. Zhu, S. Rao, S. Xu, Y. Huang, F. Liu, X. Feng, W. Zhang, *Laser Photonics Rev.* **2022**, *16*, 2100663.
[20] Y. K. R. Wu, A. E. Hollowell, C. Zhang, L. J. Guo, *Sci. Rep.* **2013**, *3*, 2013
[21] C. Yang, W. Shen, J. Zhou, X. Fang, D. Zhao, X. Zhang, C. Ji, B. Fang, Y. Zhang, X. Liu, L. J. Guo, *Adv. Opt. Mater.* **2016**, *4*, 1981.
[22] M. A. Kats, R. Blanchard, P. Genevet, F. Capasso, *Nat. Mater.* **2013**, *12*, 20.
[23] K. T. Lee, S. Seo, J. Y. Lee, L. J. Guo, *Adv. Mater.* **2014**, *26*, 6324.
[24] C. Yang, W. Shen, Y. Zhang, K. Li, X. Fang, X. Zhang, X. Liu, *Sci. Rep.* **2015**, *5*, 9285.
[25] K. Mao, W. Shen, C. Yang, X. Fang, W. Yuan, Y. Zhang, X. Liu, *Sci. Rep.* **2016**, *6*, 19289.
[26] I. G. de Souza, V. F. Rodriguez-Esquerre, D. F. Rêgo, *Appl. Opt.* **2018**, *57*, 6755.
[27] S. So, J. Mun, J. Park, J. Rho, *Adv. Mater.* **2023**, *35*, 2206399.
[28] C. Lee, G. Chang, J. Kim, G. Hyun, G. Bae, S. So, J. Yun, J. Seong, Y. Yang, D. Y. Park, S. Jeon, J. Rho, *ACS Photonics* **2022**, *10*, 919.

[29] D. Sell, J. Yang, S. Doshay, R. Yang, J. A. Fan, *Nano Lett.* **2017**, *17*, 3752.
[30] T. Phan, D. Sell, E. W. Wang, S. Doshay, K. Edee, J. Yang, J. A. Fan, *Light Sci. Appl.* **2019**, *8*, 48.
[31] M. Mansouree, A. McClung, S. Samudrala, A. Arbabi, *ACS Photonics* **2021**, *8*, 455.
[32] M. Zhou, D. Liu, S. W. Belling, H. Cheng, M. A. Kats, S. Fan, M. L. Povinelli, Z. Yu, *ACS Photonics* **2021**, *8*, 2265.
[33] Z. Liu, D. Zhu, S. P. Rodrigues, K. T. Lee, W. Cai, *Nano Lett.* **2018**, *18*, 6570.
[34] I. Tanriover, W. Hadibrata, J. Scheuer, K. Aydin, *Opt. Express* **2021**, *29*, 27219.
[35] A. Lininger, M. Hinczewski, G. Strangi, *ACS Photonics* **2021**, *8*, 3641.
[36] X. Lu, W. Li, Z. Zhu, Y. Hu, Z. Tang, W. Zhang, K. Liu, Y. Su, J. Zheng, W. Chen, M. Tang, Z. Xie, Y. Huang, L. Li, *Adv. Theory Simul.* **2022**, *5*, 2100338.
[37] M. Zhelyeznyakov, J. Fröch, A. Wirth-Singh, J. Noh, J. Rho, S. Brunton, A. Majumdar, *Commun. Eng.* **2023**, *2*, 60.
[38] I. Kim, H. Kim, S. Han, J. Kim, Y. Kim, S. Eom, A. Barulin, I. Choi, J. Rho, L. P. Lee, *Adv. Mater.* **2023**, *35*, 2300229.
[39] Z. Lin, R. Pestourie, C. Roques-Carmes, Z. Li, F. Capasso, M. Soljacic, S. G. Johnson, *Opt. Express* **2022**, *30*, 28358.
[40] Z. Shen, F. Zhao, C. Jin, S. Wang, L. Cao, Y. Yang, *Nat. Commun.* **2023**, *14*, 1035.
[41] X. He, Y. Liu, K. Ganesan, A. Ahnood, P. Beckett, F. Eftekhari, D. Smith, M. H. Uddin, E. Skafidas, A. Nirmalathas, R. R. Unnithan, *APL Photonics* **2020**, *5*, 046104.
[42] J. P. Hugonin, P. Lalanne, Light-in-complex-nanostructures/RETICOLO: V9 (Version 9). Zenodo, https://doi.org/10.5281/zenodo.4419063, (accessed: November 2022).
[43] M. G. Moharam, T. K. Gaylord, *J. Opt. Soc. Am.* **1981**, *71*, 811.
[44] W. M. Hayness, D. R. Lide, *CRC Handbook of Chemistry and Physics*, CRC Press, Boca Raton, Florida **2014**.
[45] H. Song, Y. Ma, Y. Han, W. Shen, W. Zhang, Y. Li, X. Liu, Y. Peng, X. Hao, *Adv. Theory Simul.* **2021**, *4*, 2000299.
[46] C. Kim, D. Park, H. N. Lee, *Sensors* **2020**, *20*, 594.
[47] X. Lin, Y. Liu, J. Wu, Q. Dai, *ACM Trans. Graph.* **2014**, *33*, 233.
[48] K.-T. Lee, J.-Y. Jang, S. J. Park, C. Ji, S.-M. Yang, L. J. Guo, H. J. Park, *Adv. Opt. Mater.* **2016**, *4*, 1696.
[49] J. C. Liang, Q. Cheng, Y. Gao, C. Xiao, S. Gao, L. Zhang, S. Jin, T. J. Cui, *IEEE Trans. Antennas Propag.* **2022**, *70*, 8798.
[50] Z. Lou, Q. Wang, X. Zhou, U. I. Kara, R. S. Mamtani, H. Lv, M. Zhang, Z. Yang, Y. Li, C. Wang, S. Adera, X. Wang, *J. Mater. Sci. Technol.* **2022**, *113*, 33.